DOI: 10.61782/fa.2023.0285

forum acusticum 2023

DISCONTINUOUS GALERKIN METHODS FOR THE ACOUSTIC CONSERVATION EQUATIONS WITH APPLICATION TO AEROACOUSTIC

Johannes Heinz*
TU Wien
Institute of Mechanics and Mechatronics

Manfred Kaltenbacher
TU Graz
Institute of Fundamentals and Theory
in Electrical Engineering

ABSTRACT

The acoustic conservation equations are a subset of the compressible flow equations and describe the generation and propagation of acoustic waves by the two acoustic primary variables: acoustic pressure and acoustic particle velocity. Therefore, the equations (an exact reformulation of the APE-2) can be natively used in the context of hybrid aeroacoustic. In order to achieve a stable finite element (FE) approximation by the continuous Galerkin method, these two physical quantities have to be defined in different Sobolev spaces to fulfill the Ladyzhenskaya–Babuška–Brezzi condition. Another approach is to apply the Discontinuous Galerkin (DG) method, which enforces coupling between elements via numerical fluxes in surface integrals only and thus has advantages regarding computational efficiency. We present a high-order DG formulation that yields optimal spatial and temporal convergence rates and provide implementational details in the context of hybrid aeroacoustics. Furthermore, the application to an aeroacoustic test case demonstrates the developed DG approach's suitability for aeroacoustic computations.

Keywords: *acoustic conservation equations, high-order finite elements, discontinuous Galerkin methods, hybrid aeroacoustics*

**Corresponding author*: *johannes.heinz@tuwien.ac.at.*

1. INTRODUCTION

We propose a hybrid aeroacoustic solver for low Mach numbers that is fully based on DG discretization. The optimal rates of convergence for used incompressible flow solver `ExaDG` has been shown in [1]. The solver renders fast and memory efficient [2] by using matrix-free operator evaluations [3].

The acoustic DG solver discussed within this work uses the same matrix-free implementations provided by `deal.II` [4], and will be publically available through `ExaDG`.

We made several design decisions to avoid usual bottlenecks: Input/Output (I/O) operations should be kept to a minimum in high-performance computing [5]. Therefore, we solve fluid and acoustic simulations side by side and skip the expensive I/O. This methodology has another advantage: Back-coupling from acoustic to fluid can be easily considered using the feedback term proposed in [6]. Acoustic scales are much larger than fluid scales. Thus, we use a much coarser mesh for acoustic, also known as the grid-splitting technique [7]–[11]. Using much coarser meshes for acoustic than fluid requires *conservative interpolation* of acoustic sources from the fluid grid to the acoustic grid. To avoid expensive grid intersection operations, we use a conservative cell-volume weighted interpolation methodology [12].

Within this work, we show the convergence rates for the acoustic solver and apply the acoustic solver in the context of hybrid aeroacoustics.

2. GOVERNING EQUATIONS

Within this work we are solving the acosutic conservation equations

$$\frac{\partial \boldsymbol{u}}{\partial t} + \frac{1}{\rho}\nabla p = \boldsymbol{0} \quad \text{on } \Omega, \tag{1}$$

$$\frac{\partial p}{\partial t} + \rho c^2 \nabla \cdot \boldsymbol{u} = c^2 f = -\frac{\partial p_{\text{cfd}}}{\partial t} \quad \text{on } \Omega, \tag{2}$$

with suitable boundary conditions (BCs)

$$p = g_p \quad \text{on } \partial\Omega_p^{\text{D}}, \tag{3}$$

$$\boldsymbol{u} \cdot \boldsymbol{n} = 0 \quad \text{on } \partial\Omega^{\text{ref}}, \tag{4}$$

$$\rho c \boldsymbol{u} \cdot \boldsymbol{n} = p \quad \text{on } \partial\Omega^{\text{abc}}. \tag{5}$$

Here, the acoustic pressure is p, the acoustic particle velocity is $\boldsymbol{u}$, the speed of sound is c, and ρ is the mean density of the fluid. It is possible to prescribe pressure Dirichlet boundary conditions Eqn. (3) (BCs), sound hard BCs Eqn. (4), and first oder absorbing BCs Eqn. (5) (ABCs) [13]. A body force term f introduces acoustic sources in the equations. In the context of aeroacoustic these source terms are defined as the temporal derivative of the incompressible hydrodynamic pressure p_{cfd}, which is obtained by solving the incompressible Navier–Stokes equations, see [7], [14]. The convected form of the equations under consideration can be seen as an exact reformulation of the Acoustic Perturbation Equations (APE-2) [7] which has been introduced by [14]. Within this work, we completely neglect convection; in this sense, we consider Ribner's dilatation equation [15] in the first order form.

3. NOTATION

A physical domain Ω is approximated by a computational domain Ω_h. The boundary of the computational domain is Γ_h. The computational domain is subdivided into finite elements with Lagrange shape functions of order k. Integration is performed by means of Legendre–Gauss–Lobatto quadrature with $n_q = k+1$ integration points. Information inside an element is denoted with superscript $-$; information in adjacent elements is denoted with superscript $+$. If no superscript is provided, we implicitly assume that information is defined inside elements.

The acoustic pressure p and acoustic particle velocity $\boldsymbol{u}$ is defined in the L2 space, and thus, its approximation is continuous inside elements and discontinuous between elements. On faces, elements are coupled with numerical fluxes which are indicated by superscript $*$. Given an arbitrary quantity b, the averaging operator $\{\!\{b\}\!\} = (b^- + b^+)/2$, jump operator $[b] = b^- - b^+$, and normal jump operator $[\![b]\!] = b^- \otimes \boldsymbol{n}^- + b^+ \otimes \boldsymbol{n}^+$ are defined using the notation introduced in [16], [17].

Integrals are abbreviated by $(b, b)_{\Omega_e} = \int_{\Omega_e} b \cdot b \ \mathrm{d}\Omega$ and $(b, b)_{\partial\Omega_e} = \int_{\partial\Omega_e} b \cdot b \ \mathrm{d}\Gamma$, with inner products indicated by $\cdot$.

4. SPATIAL DISCRETIZATION

The semi-discrete system of equations is obtained by multiplication with corresponding test functions q_h and $\boldsymbol{w}_h$ and two integraions by parts

$$\left(q_h, \frac{1}{c^2}\frac{\partial p_h}{\partial t}\right)_{\Omega_e} + (q_h, \rho \nabla \cdot \boldsymbol{u}_h)_{\Omega_e} - (q_h \boldsymbol{n}, \rho(\boldsymbol{u}_h^* - \boldsymbol{u}_h))_{\partial\Omega_e} = (q_h, f)_{\Omega_e}, \tag{6}$$

$$\left(\boldsymbol{w}_h, \rho\frac{\partial \boldsymbol{u}_h}{\partial t}\right)_{\Omega_e} + (\boldsymbol{w}_h, \nabla p_h)_{\Omega_e} - (\boldsymbol{w}_h \cdot \boldsymbol{n}, p_h^* - p_h)_{\partial\Omega_e} = \boldsymbol{0}. \tag{7}$$

We use the well-known Lax-Friedrichs fluxes

$$p_h^* = \{\!\{p_h\}\!\} + \tau\, [\![\boldsymbol{u}_h]\!], \tag{8}$$

$$\boldsymbol{u}_h^* = \{\!\{\boldsymbol{u}_h\}\!\} + \gamma\, [\![p_h]\!], \tag{9}$$

with penalty parameters that are only defined on the unterlying materials properties $\tau = \frac{\rho c}{2}$ and $\gamma = \frac{1}{2\rho c}$ [18]–[21]. Note that we apply BCs weakly through the mirror principle, cf. [22].

5. TEMPORAL DISCRETIZATION

Governing equations in matrix notation read

$$\mathbb{M}\frac{\partial \boldsymbol{U}_h}{\partial t} + \mathbb{K}\boldsymbol{U}_h = \boldsymbol{F}_h, \tag{10}$$

with matrices $\mathbb{M}$ and $\mathbb{K}$ as well as global DoF vectors containing pressure and velocity contributions $\boldsymbol{U}_h$ and the source terms $\boldsymbol{F}_h$. This way we can write the Jth order Backward Differentiation Formula (BDF) time integraion scheme as

$$\mathbb{M}\frac{\gamma_0 \boldsymbol{U}^{n+1} + \sum_{i=0}^{J-1} \alpha_i \boldsymbol{U}^{n-i}}{\Delta t} + \mathbb{K}\boldsymbol{U}^{n+1} = \boldsymbol{F}_h^{n+1}, \tag{11}$$

with the BDF coefficients γ_0 and α; the coefficients for adaptive time-stepping can be found in [23].

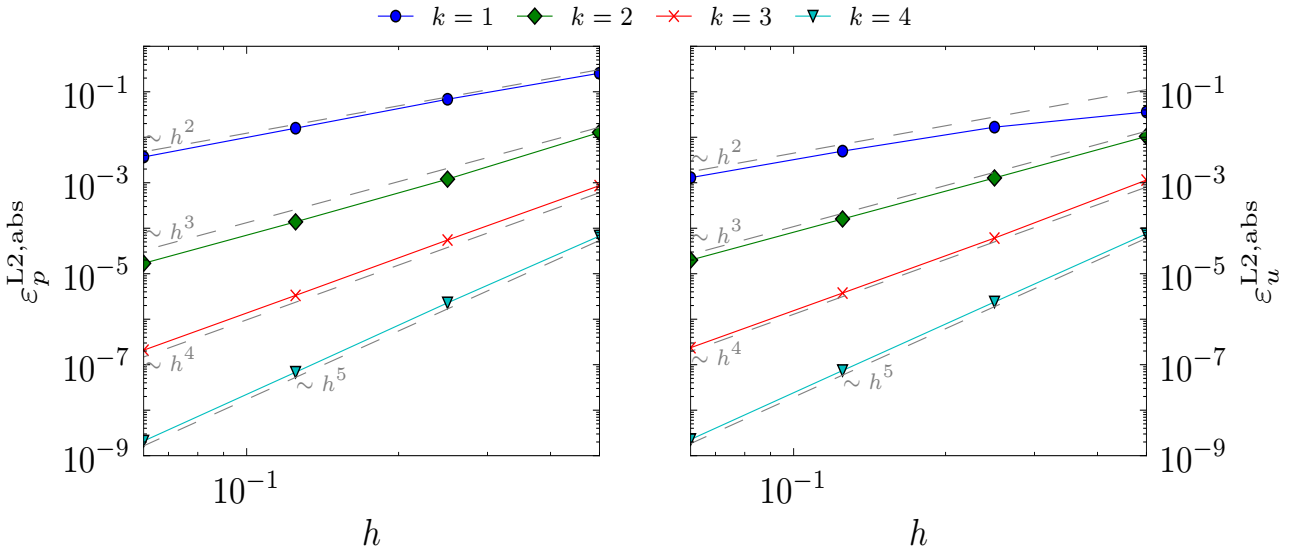

Figure 1. Spatial rates of convergence for polynomial degree k. Optimal rates $k+1$ are obtained.

6. ACOUSTIC CONVERGENCE STUDY

To be able to benchmark the discretizations agains an analytical solution we are using the test case of a vibrating membrane. This test case was also considered amongst others in [19], [24], [25]. In two dimension and with $c = 1\mathrm{ms}^{-1}$ and $\rho = 1\mathrm{kgm}^{-3}$ it reads

$$p_{\mathrm{ana}} = \cos(\sqrt{2}\pi t)\sin(\pi x_1)\sin(\pi x_2), \tag{12}$$

$$\boldsymbol{u}_{\mathrm{ana}} = -\frac{\sin(\sqrt{2}\pi t)}{\sqrt{2}}\begin{pmatrix}\cos(\pi x_1)\sin(\pi x_2)\\ \cos(\pi x_2)\sin(\pi x_1)\end{pmatrix}. \tag{13}$$

We are comparing absolute L2 errors for pressure

$$\varepsilon_p^{\mathrm{L2,abs}} = \sqrt{\int_\Omega (p_h - p_{\mathrm{ana}})^2 \ \mathrm{d}\Omega}, \tag{14}$$

and similarely for velocity after $t = 1\mathrm{s}$.

The computational domain is a square $\Omega_h = [0\mathrm{m}, 1\mathrm{m}]^2$. Within the investigation we use homogenous pressure Dirichlet BCs. For the spatial convergence study we are using a time step based on the CFL condition

$$\Delta t = \frac{\mathrm{Cr}}{k^{1.5}}\frac{h}{c}, \tag{15}$$

where h is the minimal element edge length and the exponent 1.5 is motivated by [26]. The Courant number is chosen $\mathrm{Cr} = 0.01$ in combination with time integration order $J = 4$. Corresponding results are plotted in Fig. 1 and we can observe optimal spatial rates of convergence $k+1$.

For the temporal convergence study we are using polynomial degree $k = 7$ and $h = 0.125\mathrm{m}$. As shown in Fig. 2 we obtain minimally optimal temoporal rates of convergence J. For the velocity with BDF1 and the pressure with BDF2 we observe superconvergence. Nevertheless, looking at the combination of pressure and velocity we obtain optimal rates of conergence. Superconvergence is not expected and seems to be related to the test case since we could not observe superconvergence in other test cases.

7. AEROACOUSTIC VOLUME COUPLING

We are considering no convection and no back-coupling of the acoustic to the fluid. Therefore, the coupling reduces to two operations: computation of the source term and interpolation to the acoustic grid.

For the computation of the temporal derivative of the hydrodynamic pressure we are using a Jth order BDF scheme

$$\frac{\partial p_{\mathrm{cfd}}}{\partial t} \approx \frac{\gamma_0 p_{h,\mathrm{cfd}}^{n+1} - \sum_{i=0}^{J-1}\alpha_i p_{h,\mathrm{cfd}}^{n-i}}{\Delta t}, \tag{16}$$

This operation is performed on the fluid grid. Within this work $J = 2$.

As shown in multiple publications, see, e.g., [27], [28], a consservative interpolation is key in computational aeroacoustic with grid-splitting.

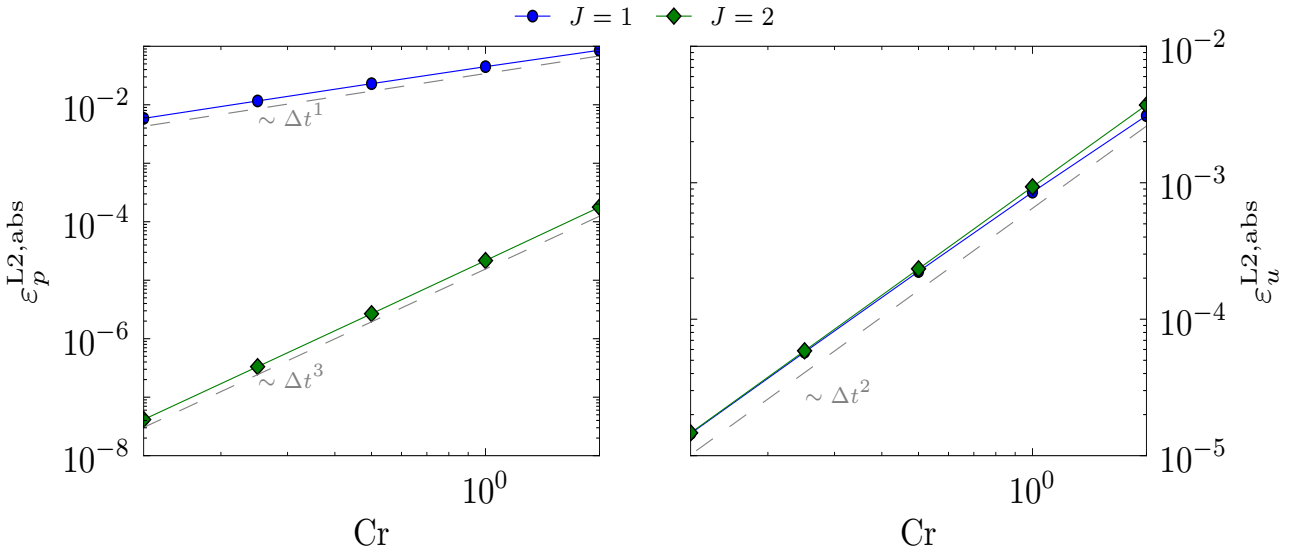

Figure 2. Temporal rates of convergence for time integration scheme. In some cases we unexpectedly obsever super-convergence but we have at least the expected optimal rates of order J. Optimal rates J are obtained.

Within our solver we generalized the fully conservative cell-volume weight interpolation methodology from [12] to high-orders DG schemes of the CFD solver. Note that this interpolation scheme is particularily efficient since no grid intersections have to be computed. The integration and interpolation of the source term is performed as follows:

1. Compute *and* integrate source term on fluid grid.
2. Fetch DoF positions of fluid grid.
3. Search corresponding cells and reference points on the acoustic grid $\boldsymbol{\xi}$.
4. At every $\boldsymbol{\xi}$: Evaluate shape functions of locally relevant acoustic DoFs, multiply by corresponding value of the integrated source term from the fluid grid, and assemble to global acoustic source vector $\boldsymbol{F}_h$.

In our implementations this procedure works for arbitrary orders of fluid and acoustic simulations.

8. NUMERICAL RESULTS

To demonstrate the solver in the context of aeroacoustic we are considering a cylinder of radius $r = 0.01\mathrm{m}$ in a cross-flow with velocity $\bar{\boldsymbol{u}}_{\mathrm{cfd}} = (10, 0)^T \mathrm{ms}^{-1}$. The material parameters are $\nu = 0.001\mathrm{m}^2\mathrm{s}^{-1}$, $c = 343.5\mathrm{ms}^{-1}$, $\rho = 1.204\mathrm{kgm}^{-3}$. The CFD domain is a rectangle, which spans from $(-0.5\mathrm{m}, -0.2\mathrm{m})^T \times (0.5\mathrm{m}, 0.2\mathrm{m})^T$, with a cylindrical hole and consists of 448 elements with polynomial degree 4 for the velocity and 3 for the pressure (29568 DoFs). At the left side inflow boundary conditions with the constant velocity $\bar{\boldsymbol{u}}_{\mathrm{cfd}}$ are used. At the right side pressure outflow boundary consditions are prescribed, and at top and bottom symmetric BCs are used. The acoustic domain is a shell with outer radius $R = 10\mathrm{m}$ and innter radius r. Inner boundaries are modeled sound hard and at outer boundaries first order ABCs are used. Different configurations for the spatial discretization are listed in Tab. 1. The time step size is chosen adaptively with a

Table 1. Different spatial discretizations of acoustic. C is used to distinguis between configurations.

C	k	elements	DoFs
1	2	84	2268
2	3	84	4032
3	3	324	15552
4	3	5124	245952
5	3	20484	983232

Courant number of $\mathrm{Cr} = 0.8$ for the CFD and is limited by a maximal time step size of $\Delta t = 12.5 \times 10^{-6}\mathrm{s}$. The

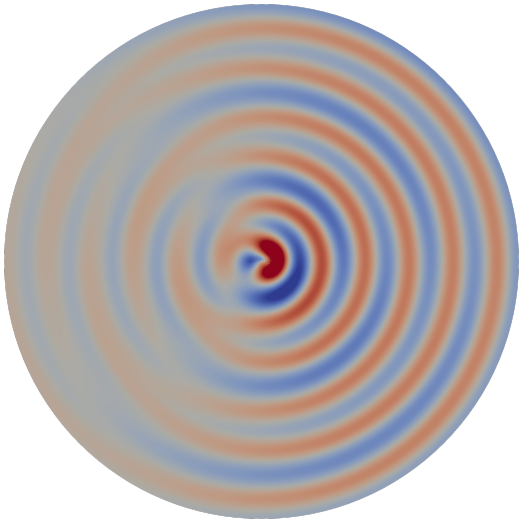

Figure 3. Acoustic pressure field of cylinder in cross-flow at $t = 0.446$s for configuration C4.

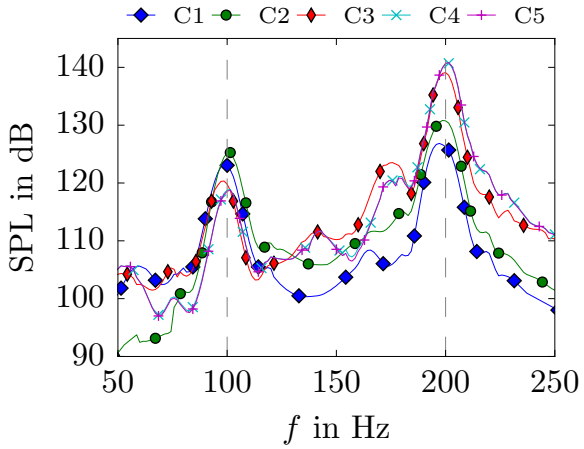

Figure 4. Simulation results for different configurations listed in Tab. 1.

acoustic pressure field is depicted in Fig. 3 for configuration C4.

Fig. 4 shows the spectrum of the acoustic sound pressure level (SPL)

$$\mathrm{SPL} = 20 \log_{10} \left(\frac{p}{p_0} \right), \tag{17}$$

at $\boldsymbol{x} = (0, 4\mathrm{m})^T$, with $p_0 = 20 \times 10^{-6}$Pa. The same frequencies at which modes occur are predicted independent of the discretization. The main difference is in the obtained amplitudes; a finer discretization yields greater amplitudes for high frequencies since less numerical dissipation is present. On the other hand, the SPL at the shedding frequency (100Hz) is overestimated by the coarse discretization. Note that C4 and C5 yield the same results, indicating that the acoustic solver converged to the optimal values. Therefore, better results can only be expected for a finer CFD simulation. It sticks out that obtained results are reasonable, even for very coarse discretizations.

9. CONCLUSION

We presented a hybrid aeroacoustic solver for low Mach numbers with high-performance computing in mind. Used incompressible flow solver shows optimal rates of convergence [1]. The spatial discretization of the acoustic solver show expected optimal rates of convergence in space. For the temporal discretization, we also obtain optimal convergence rates (in rare cases, for the vibrating membrane test case, we even see superconvergence). Both solvers employ high-order DG methods. The volume coupling between a fine fluid grid and a coarser acoustic grid is performed using a fully conservative cell-volume weighted interpolation methodology, which avoids any computation of grid intersections and works for arbitrary polynomial degrees of both, the CFD solver as well as the acoustic solver. Applying the solver to the test case of a cylinder in a cross-flow yields good results already for extremely coarse discretizations of the acoustic.

10. ACKNOWLEDGMENTS

This project has received funding from the European Union's Framework Programme for Research and Innovation Horizon 2020 (2014-2020) under the Marie Skłodowska–Curie Grant Agreement No. [812719].
The authors acknowledge collaboration with Niklas Fehn, Martin Kronbichler, and Peter Munch as well as the `deal.II` community.
Special thanks to Florian Kraxberger, Paul Maurerlehner, and Andreas Wurzinger for several valuable discussions on hybrid aeroacoustics.

11. REFERENCES

[1] N. Fehn, W. A. Wall, and M. Kronbichler, "On the stability of projection methods for the incompressible Navier-Stokes equations based on high-order discontinuous Galerkin discretizations," *Journal of Computational Physics*, vol. 351, pp. 392–421, 2017, ISSN: 0021-9991. DOI: https://doi.org/10.1016/j.jcp.2017.09.031.

[2] ——, "Efficiency of high-performance discontinuous Galerkin spectral element methods for under-resolved turbulent incompressible flows," *International Journal for Numerical Methods in Fluids*, vol. 88, no. 1, pp. 32–54, 2018. DOI: 10.1002/fld.4511.

[3] M. Kronbichler and K. Kormann, "Fast matrix-free evaluation of discontinuous Galerkin finite element operators," *ACM Trans. Math. Softw.*, vol. 45, no. 3, 2019, ISSN: 0098-3500. DOI: 10.1145/3325864.

[4] D. Arndt, W. Bangerth, M. Feder, M. Fehling, R. Gassmöller, T. Heister, L. Heltai, M. Kronbichler, M. Maier, P. Munch, J.-P. Pelteret, S. Sticko, B. Turcksin, and D. Wells, "The deal.II library, version 9.4," *Journal of Numerical Mathematics*, 2022, Accepted. DOI: 10.1515/jnma-2022-0054.

[5] D. Kempf and C.-D. Munz, "Zonal direct-hybrid aeroacoustic simulation of trailing edge noise using a high-order discontinuous Galerkin spectral element method," *Acta Acustica*, vol. 6, p. 39, 2022. DOI: https://doi.org/10.1051/aacus/2022030.

[6] R. Ewert and J. Kreuzinger, "Hydrodynamic/acoustic splitting approach with flow-acoustic feedback for universal subsonic noise computation," *Journal of Computational Physics*, vol. 444, p. 110 548, 2021. DOI: 10.1016/j.jcp.2021.110548.

[7] A. Hüppe and M. Kaltenbacher, "Comparison of source term formulations for computational aeroacoustics," in *19th AIAA/CEAS Aeroacoustics Conference*, American Institute of Aeronautics and Astronautics, 2013. DOI: 10.2514/6.2013-2170.

[8] J.-H. Seo and Y. J. Moon, "Perturbed compressible equations for aeroacoustic noise prediction at low Mach numbers," *AIAA Journal*, vol. 43, no. 8, pp. 1716–1724, 2005. DOI: 10.2514/1.3001.

[9] S. Schoder, C. Junger, M. Weitz, and M. Kaltenbacher, "Conservative source term interpolation for hybrid aeroacoustic computations," in *25th AIAA/CEAS Aeroacoustics Conference*, American Institute of Aeronautics and Astronautics, 2019. DOI: 10.2514/6.2019-2538.

[10] S. Schoder, K. Roppert, M. Weitz, C. Junger, and M. Kaltenbacher, "Aeroacoustic source term computation based on radial basis functions," *International Journal for Numerical Methods in Engineering*, vol. 121, no. 9, pp. 2051–2067, 2020. DOI: 10.1002/nme.6298.

[11] P. Maurerlehner, S. Schoder, C. Freidhager, A. Wurzinger, A. Hauser, F. Kraxberger, S. Falk, S. Kniesburges, M. Echternach, M. Döllinger, and M. Kaltenbacher, "Efficient numerical simulation of the human voice," *Elektrotechnik & Informationstechnik*, vol. 138, no. 3, pp. 219–228, 2021. DOI: 10.1007/s00502-021-00886-1.

[12] M. Kaltenbacher, M. Escobar, S. Becker, and I. Ali, "Numerical simulation of flow-induced noise using LES/SAS and Lighthill's acoustic analogy," *International Journal for Numerical Methods in Fluids*, n/a–n/a, 2009. DOI: 10.1002/fld.2123.

[13] B. Engquist and A. Majda, "Absorbing boundary conditions for the numerical simulation of

waves," *Mathematics of Computation*, vol. 31, no. 139, pp. 629–651, 1977. DOI: 10.1090/s0025-5718-1977-0436612-4.

[14] R. Ewert and W. Schröder, "Acoustic perturbation equations based on flow decomposition via source filtering," *Journal of Computational Physics*, vol. 188, no. 2, pp. 365–398, 2003. DOI: 10.1016/s0021-9991(03)00168-2.

[15] H. Ribner, "The generation of sound by turbulent jets," pp. 103–182, 1964. DOI: 10.1016/s0065-2156(08)70354-5.

[16] F. Bassi, A. Crivellini, D. D. Pietro, and S. Rebay, "An artificial compressibility flux for the discontinuous Galerkin solution of the incompressible Navier–Stokes equations," *Journal of Computational Physics*, vol. 218, no. 2, pp. 794–815, 2006, ISSN: 0021-9991. DOI: https://doi.org/10.1016/j.jcp.2006.03.006.

[17] F. Bassi, A. Crivellini, D. A. D. Pietro, and S. Rebay, "An implicit high-order discontinuous Galerkin method for steady and unsteady incompressible flows," *Computers & Fluids*, vol. 36, no. 10, pp. 1529–1546, 2007, Special Issue Dedicated to Professor Michele Napolitano on the Occasion of his 60th Birthday, ISSN: 0045-7930. DOI: https://doi.org/10.1016/j.compfluid.2007.03.012.

[18] R. J. LeVeque, *Finite Volume Methods for Hyperbolic Problems*. Cambridge: Cambridge University Press, 2002. DOI: 10.1017/cbo9780511791253.

[19] N. Nguyen, J. Peraire, and B. Cockburn, "High-order implicit hybridizable discontinuous Galerkin methods for acoustics and elastodynamics," *Journal of Computational Physics*, vol. 230, no. 10, pp. 3695–3718, 2011, ISSN: 0021-9991. DOI: https://doi.org/10.1016/j.jcp.2011.01.035.

[20] M. Hochbruck, T. Pažur, A. Schulz, E. Thawinan, and C. Wieners, "Efficient time integration for discontinuous Galerkin approximations of linear wave equations," *ZAMM - Journal of Applied Mathematics and Mechanics / Zeitschrift für Angewandte Mathematik und Mechanik*, vol. 95, no. 3, pp. 237–259, 2014. DOI: 10.1002/zamm.201300306.

[21] M. Kronbichler, S. Schoeder, C. Müller, and W. A. Wall, "Comparison of implicit and explicit hybridizable discontinuous Galerkin methods for the acoustic wave equation," *International Journal for Numerical Methods in Engineering*, vol. 106, no. 9, pp. 712–739, 2016. DOI: 10.1002/nme.5137.

[22] J. S. Hesthaven and T. Warburton, *Nodal Discontinuous Galerkin Methods*. Springer, New York, NY, 1, 2008, ISBN: 978-0-387-72065-4. DOI: 10.1007/978-0-387-72067-8.

[23] N. Fehn, J. Heinz, W. A. Wall, and M. Kronbichler, "High-order arbitrary Lagrangian–Eulerian discontinuous Galerkin methods for the incompressible Navier–Stokes equations," *Journal of Computational Physics*, vol. 430, p. 110 040, 2021, ISSN: 0021-9991. DOI: 10.1016/j.jcp.2020.110040.

[24] C. Courtès, E. Franck, P. Helluy, and H. Oberlin, "Study of physics-based preconditioning with high-order Galerkin discretization for hyperbolic wave problems," *ESAIM: Proc. and Surveys*, vol. 55, E. Frénod, E. Maitre, A. Rousseau, S. Salmon, and M. Szopos, Eds., pp. 61–82, 2016. DOI: 10.1051/proc/201655061.

[25] S. Schoeder, W. Wall, and M. Kronbichler, "ExWave: A high performance discontinuous Galerkin solver for the acoustic wave equation," *SoftwareX*, vol. 9, pp. 49–54, 2019, ISSN: 2352-7110. DOI: https://doi.

org/10.1016/j.softx.2019.01.001.

[26] N. Fehn, W. A. Wall, and M. Kronbichler, "Robust and efficient discontinuous Galerkin methods for under-resolved turbulent incompressible flows," *Journal of Computational Physics*, vol. 372, pp. 667–693, 2018, ISSN: 0021-9991. DOI: 10.1016/j.jcp.2018.06.037.

[27] S. Schoder, C. Junger, M. Weitz, and M. Kaltenbacher, "Conservative source term interpolation for hybrid aeroacoustic computations," 2019. DOI: 10.2514/6.2019-2538.

[28] S. Schoder, A. Wurzinger, C. Junger, M. Weitz, C. Freidhager, K. Roppert, and M. Kaltenbacher, "Application limits of conservative source interpolation methods using a low mach number hybrid aeroacoustic workflow," *Journal of Theoretical and Computational Acoustics*, vol. 29, no. 01, p. 2 050 032, 2021. DOI: 10.1142/s2591728520500322.

[29] D. Arndt, N. Fehn, G. Kanschat, K. Kormann, M. Kronbichler, P. Munch, W. A. Wall, and J. Witte, "ExaDG: High-order discontinuous Galerkin for the exa-scale," in *Software for Exascale Computing - SPPEXA 2016-2019*, H.-J. Bungartz, S. Reiz, B. Uekermann, P. Neumann, and W. E. Nagel, Eds., Cham: Springer International Publishing, 2020, pp. 189–224.